Inorganic Chemistry

Article

pubs.acs.org/IC

Polymorph Control of Luminescence Properties in Molecular Crystals of a Platinum and Organoarsenic Complex and Formation of Stable One-Dimensional Nanochannel

Hikaru Unesaki,[†] Takuji Kato,[†] Seiji Watase,[‡] Kimihiro Matsukawa,[‡] and Kensuke Naka*[,†]

[†]Department of Chemistry and Materials Technology, Graduate School of Science and Technology, Kyoto Institute of Technology, Goshokaido-cho, Matsugasaki, Sakyo-ku, Kyoto 606-8585, Japan

[‡]Osaka Municipal Technical Research Institute, 1−6-50 Morinomiya, Joto-ku, Osaka 536−8533, Japan

Supporting Information

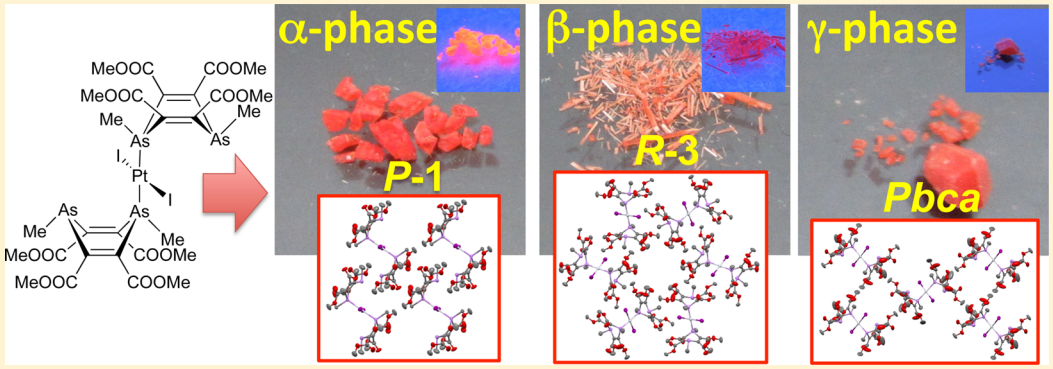

ABSTRACT: The mononuclear diiodoplatinum(II) complex (*trans*-PtI_2(*cis*-DHDAMe)$_2$), where *cis*-DHDAMe = *cis*-1,4-dihydro-1,4-dimethyl-2,3,5,6-tetrakis(methoxycarbonyl)-1,4-diarsinine, forms three different crystalline polymorphs that can be either concomitantly or separately obtained on varying the recrystallization conditions. Cubic red crystals (*α*-phase) and red-orange needles (*β*-phase) exhibit solid-state red emissions at room temperature. Cubic red crystals of the *γ*-phase show no solid-state emission at room temperature. All crystalline structures were confirmed by X-ray crystallography. Room-temperature strongly luminescent crystals (*α*-phase) (λ_{em} = 657 nm, Φ = 0.52) have a triclinic $P\bar{1}$ (No. 2) structure and no voids in the crystal structure. Red-orange needle-shaped crystals of the *β*-phase exhibit moderate red luminescence (λ_{em} = 695 nm, Φ = 0.09) at room temperature and have a trigonal, $R\bar{3}$ (No. 148), structure. In the needlelike crystals of the *β*-phase, stable hexagonal arrays of nanoporous channels, 5.0 Å in diameter, are formed. Room-temperature nonluminescent crystals (*γ*-phase) have an orthorhombic, *Pbca* (No. 61), structure with a void volume that is 4.9% of the total crystal volume. After heating the *α*-phase crystals at 150 °C for 2 min, a powder XRD pattern different from the original crystal is obtained, and its solid-state emission at room temperature decreased. After heating the *β*-phase crystals at 150 °C for 2 min, the emission wavelength and the quantum yield of the solid-state emission at room temperature and the powder XRD pattern are the same as those of the *α*-phase after heating at 150 °C. A crystal-to-crystal transition triggered by the thermal stimulus produces a different stable polymorph of the mononuclear diiodoplatinum(II) complex. The one-dimensional nanoporous crystals encapsulated iodine without distorting the crystal packing.

INTRODUCTION

The properties of organic and organometallic molecular materials are strongly dependent on their packing arrangement in the solid state. The manipulation and control of the molecular packing are of great importance in obtaining the desired properties and functions of the materials.[1,2] In crystal engineering, the control of polymorphism (i.e., the ability of a compound to crystallize in multiple packing arrangements) is of great interest not only for fundamental chemical knowledge but also for material technology. In such cases, the physical properties of a polymorph reflect the individual characteristics of a molecule. The network of soft interactions in the solid state can often be manipulated by crystal-to-crystal switching properties triggered by thermal, mechanical, or radiative stimuli.[3] One of the most interesting and useful properties is the control of luminescence intensities and wavelengths in a material's crystalline states.[4] However, the prediction of crystal structure is not yet entirely feasible, and it is therefore useful to develop new examples in which a given molecule will crystallize from solution in one or many crystal forms.

Received: March 10, 2014
Published: July 25, 2014

   dx.doi.org/10.1021/ic500550y | *Inorg. Chem.* 2014, 53, 8270−8277

An attractive area for crystal engineering is the control of polymorphs to construct stable one-dimensional (1D) nanochannels, because such organic supramolecular microporous solids are of interest as templates for the construction of new 1D organic optical, electrical, and magnetic materials based on functional molecular chains.[5] Although "porous coordination polymers" or " metal-organic frameworks" formed by the combination of metal ions with rigid multivalent ligands constitute the major approaches for building such solids,[6,7] other approaches for obtaining extrinsic nanoporosity result simply from crystal packing that relies on noncovalent interaction.[8,9] These nanoporous crystals are probably the most challenging approach, because such open frameworks must be maintained without the help of powerful directional bonds or pre-existing cavities, and their instability can grow after removal of the guest molecules. Such crystals are still rare among supramolecular solids.[9]

Previously, we reported on a nonporous crystalline solid consisting of an organoarsenic-Pt(II) complex (Chart 1), that

Chart 1. Structures of *trans*-PtI_2(*cis*-DHDA^{t}Bu)$_2$ and *trans*-PtI_2(*cis*-DHDAMe)$_2$

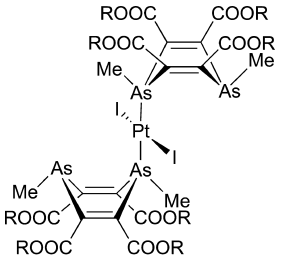

is, the mononuclear diiodoplatinum(II) complex (*trans*-PtI_2(*cis*-DHDA^{t}Bu)$_2$) with *cis*-1,4-dihydro-1,4-dimethyl-2,3,5,6-tetrakis-(*t*-butoxycarbonyl)-1,4-diarsinine (*cis*-DHDA^{t}Bu), that included solvent molecules such as CH_2Cl_2, acetone, and toluene.[10] The crystal structure was unstable after removal of the solvent molecules by heating and easily transitioned to a nonporous crystalline solid. Conformational flexibility of the bond angles around the arsenic center is an inherent property of the organoarsenic compounds.[11] The unique polymorphism might originate from the flexibility of the organoarsenic compounds. We found, as described herein, that a methoxycarbonyl-substituent analogue (Chart 1), that is, the mononuclear diiodoplatinum(II) complex (*trans*-PtI_2(*cis*-DHDAMe)$_2$) with *cis*-1,4-dihydro-1,4-dimethyl-2,3,5,6-tetrakis-(*methoxy*carbonyl)-1,4-diarsinine (*cis*-DHDAMe) forms three different crystalline polymorphs, which can be either concomitantly or separately obtained on varying the recrystallization conditions. We found that the different molecular packings in these crystals affect their solid-state emissions and that a stable crystal having a cavity-like 1D nanochannel of 5.0 Å in diameter can be obtained as one of the three polymorphs.

RESULT AND DISCUSSION

The mononuclear diiodoplatinum(II) complex (*trans*-PtI_2(*cis*-DHDAMe)$_2$) was prepared from a mononuclear dichloroplatinum(II) complex (*trans*-$PtCl_2$(*cis*-DHDAMe)$_2$) (Scheme 1).[11] The structure of the product was confirmed by X-ray crystallography (Figure 1). The perspective views of

Scheme 1. Synthesis of *trans*-PtI_2(*cis*-DHDAMe)$_2$

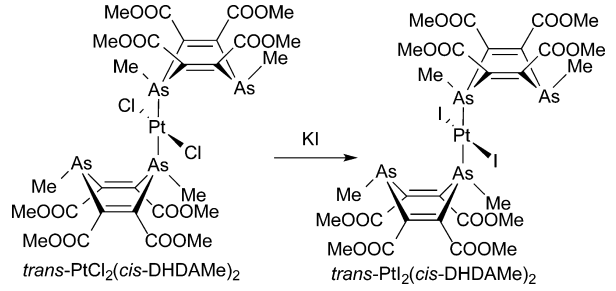

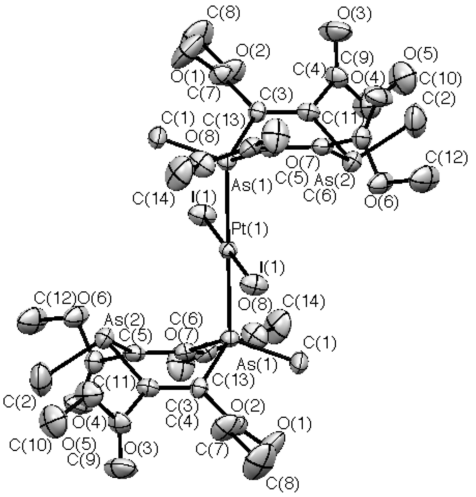

Figure 1. Perspective view of *trans*-PtI_2(*cis*-DHDAMe)$_2$ as found in the α-phase with thermal ellipsoids shown at the 50% probability level.

the complex show that the two *cis*-DHDAMe molecules are bridged with the platinum ion in an antiparallel configuration, which might be due to steric hindrance between the iodines and the methoxy groups. The mononuclear diiodoplatinum(II) complex (*trans*-PtI_2(*cis*-DHDAMe)$_2$) was recrystallized at room temperature from CH_2Cl_2 and methanol as good and poor solvents, respectively, to produce three different crystalline polymorphs depending on the recrystallization conditions (Figure 2a). When the complex is dissolved in a minimum amount of CH_2Cl_2 and a larger amount of methanol is added, cubic red crystals (α-phase) and red-orange needles (β-phase) are simultaneously formed. Both crystal forms exhibit solid-state red emissions at room temperature. The intensity of the α-phase emission is stronger than that of the β-phase. Increasing the amount of CH_2Cl_2 tends to produce the β-phase, whereas using a larger amount of CH_2Cl_2 and a minimum amount of methanol tends to form a different cubic red crystal (γ-phase), which shows no solid-state emission at room temperature.

All crystalline structures were confirmed by X-ray crystallography (Figure 2a). Room-temperature strongly luminescent crystals (α-phase) have a triclinic, $P\bar{1}$ (No. 2), structure and no voids in the crystal structure. Room-temperature nonluminescent crystals (γ-phase) have an orthorhombic, *Pbca* (No. 61), structure with a void volume that is 4.9% of the total crystal volume. Red-orange needles (β-phase) have a trigonal, $R\bar{3}$ (No. 148), structure and form a hexagonal array of nanoporous channels with 5.0 Å diameters (Figure 2b). No guest molecules were included in the crystals, as judged by ^{1}H NMR analysis. X-ray crystallographic analysis shows empty-pore hexagonal

dx.doi.org/10.1021/ic500550y | Inorg. Chem. 2014, 53, 8270−8277

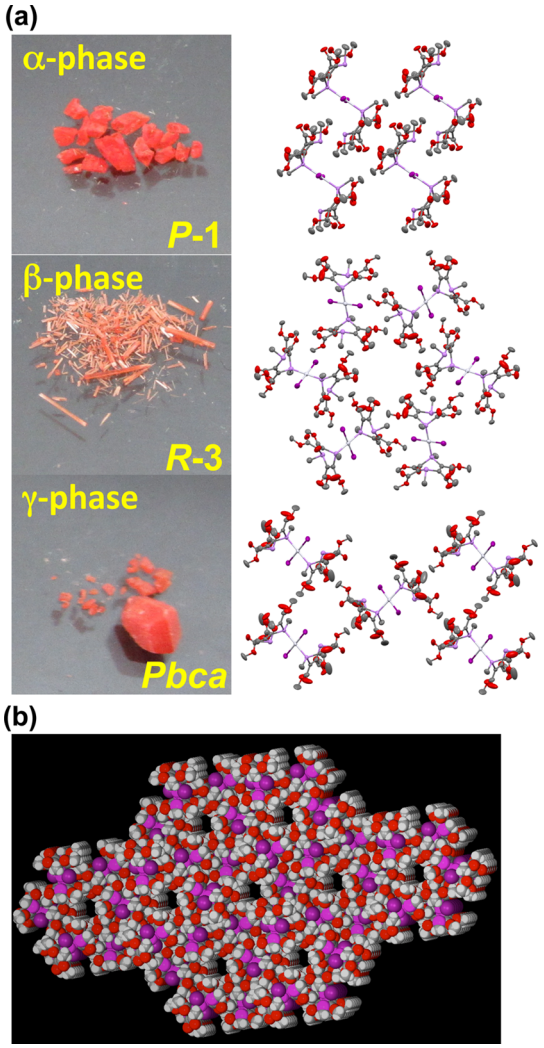

Figure 2. (a) Appearances (left) and crystal packing diagrams (right) of α-phase, β-phase, and γ-phase of *trans*-PtI_2(*cis*-DHDAMe)$_2$ (50% probability thermal ellipsoids). (b) Crystal structure of β-phase of *trans*-PtI_2(*cis*-DHDAMe)$_2$ viewed along the channel axis: a view of five layers of molecule is presented.

structures with no residual electron density in the large unoccupied volume. Weak intermolecular interactions consolidate the molecular stacks along the *a* axis and layers on the *bc* plane. The crystal density is low, and 8.5% of the volume is available to guests in the noncovalent architecture.

Selected bond length and angles for all three crystals are summarized in Table 1. No significant differences appear in the bond lengths and angles for these three crystal forms. The As−As distance of the ligand in the β-phase crystals was 0.125 and 0.127 Å longer compared with those in the α-phase and γ-phase crystals, respectively. The average As−C=C bond angle extended to 121.7° in the β-phase crystals from 119.4° in the α-phase crystals and 119.6° in the γ-phase crystals. These observations indicate increased flatness of the six-membered ring of *cis*-DHDAMe in the β-phase crystals over those in the α- and γ-phase crystals. The I−Pt−As-C torsion angle in the case of the β-form is a significant difference from those in the α-phase and γ-phase crystals (Supporting Information, Figure S3).

The α-phase crystals exhibit very intense red luminescence (λ_{em} = 657 nm) in the solid phase, even at room temperature (Figure 3). The quantum yield and luminescence decay time (Supporting Information, Figure S4) of the α-phase crystals are 0.52 and 29 μs, respectively. The needle-shaped crystals of the β-phase exhibit moderate red luminescence (λ_{em} = 695 nm) at room temperature. The quantum yield and luminescence decay time of the β-phase crystals are 0.09 and 6.8 μs, respectively. The emission spectrum of the α-phase crystals shows a band from 570 to 800 nm with a peak at 657 nm. Although onset of the emission spectrum of the β-phase crystals is the same as that of the α-phase crystals, it exhibits a broader band from 570 nm to more than 800 nm, with a peak at 695 nm. The excitation spectra of both the α-phase and β-phase crystals show similarly shaped peaks in the same region, except for a shoulder excitation peak at around 600 nm in the case of the β-phase crystals, suggesting lower-energy photoexcitation processes.

The solid-state absorption spectra of all three crystals at room temperature show almost similarly shaped peaks in the same region, suggesting similar photoexcitation processes (Figure 4a). According to the expanded absorption spectra, the position of the absorption edge for the β-phase crystals is red-shifted compared with that of the α-phase crystals (Figure 4b). The solid-state absorption of both the α-phase and β-phase crystals measured at room temperature match their excitation spectra. The absorption maxima at around 370 nm are derived from mixed metal (d_M)-to-ligand (s/p*$_{As}$)/ligand (p_{Cl})-to-ligand (s/p*$_{As}$) charge transfer (MLCT/LLCT) transitions, according to a time-dependent density functional theory (TD-DFT) calculation.[11] Because no metal−metal interaction existed in all three crystals according to the crystallographic data, the long-wavelength absorption maxima at 520 nm were assigned to spin-forbidden ^{3}MLCT transitions. The lower-energy photoexcitation processes for the β-phase crystals may be due to an increase of flatness of the six-membered ring of *cis*-DHDAMe in the β-phase crystals compared with that in the α-phase crystals.

Since the structural data rule out any specific strong intermolecular interaction in three crystal phases, the different quantum yields may be ascribed to the different local packing of the independent molecules in the three polymorphs. Although the γ-phase crystals showed no solid-state emission at room temperature, they exhibited intense emission at −196 °C without any specific shift when compared with those of the β-phase crystals at −196 °C (Supporting Information, Figure S5). In general, decreasing temperatures prevent nonradiative relaxation processes. In the recently studied aggregation-induced emission (AIE) and crystallization-induced emission (CIE) processes, luminogens are emissive in their aggregation and crystal states but nonluminescent in their solution and amorphous states. These feature shifts are triggered by the restriction of the molecular motions that blocks the nonradiative path. No emission was observed for a CH_2Cl_2 solution of *trans*-PtI_2(*cis*-DHDAMe)$_2$. The flexibility of the arsenic ligands might be a main reason for the nonluminescent properties of most of these organoarsenic complexes at room temperature even in their solid states as well as solution phases, in contrast to their phosphorus analogues. In the crystal packing of the α-phase and β-phase crystals, the methyl groups on the coordinated arsenic atoms are connected to adjacent molecules (Supporting Information, Figure S6). However, no such contact is observed in the crystal packing of the γ-phase crystals. These results suggest that the freezing of the intramolecular rotational relaxation pathways of the methyl

dx.doi.org/10.1021/ic500550y | *Inorg. Chem.* 2014, 53, 8270−8277

Table 1. Selected Distances (Å) and Angles (deg) of the Crystalline Products

		α-phase		
As···As	As(1) ···As(2)	3.260(1)		
Pt−As	Pt(1)−As(1)	2.4031(5)		
Pt−I	Pt(1)−I(1)	2.6036(4)		
C−As−C[a]	C(3)−As(1)−C(6)	98.8(2)	C(4)−As(2)−C(5)	95.3(2)
As−C═C[b]	As(1)−C(3)−C(4)	118.7(4)	As(1)−C(6)−C(5)	117.4(4)
As−C═C[c]	As(2)−C(4)−C(3)	120.5(4)	C(12)−C(10)−As(1)	121.1(2)
I−Pt−I	I(1)−Pt(1)−I(1)	180.000(16)		
As−Pt−As	As(1)−Pt(1)−As(1)	180.00(2)		
torsion angle	I(1)−Pt(1)−As(1)-C(1)	78.8(2)		
		β-phase		
As···As	As(4) ···As(5)	3.385(1)		
Pt−As	Pt(1)−As(5)	2.4065(8)		
Pt−I	Pt(1)−I(1)	2.6018(6)		
C−As−C[a]	C(3)−As(5)−C(6)	98.5(3)	C(4)−As(4)−C(5)	94.3(3)
As−C═C[b]	As(5)−C(3)−C(4)	119.8(6)	As(5)−C(6)−C(5)	118.8(5)
As−C═C[c]	As(4)−C(4)−C(3)	123.5(6)	As(4)−C(5)−C(6)	124.7(6)
I−Pt−I	I(1)−Pt(1)−I(1)	180.00(2)		
As−Pt−As	As(5)−Pt(1)−As(5)	180.00(2)		
torsion angle	I(1)−Pt(1)−As(5)−C(1)	62.9(3)		
		γ-phase		
As···As	As(1) ···As(2)	3.258(1)		
Pt−As	Pt(1)−As(1)	2.3998(7)		
Pt−I	Pt(1)−I(1)	2.5992(6)		
C−As−C[a]	C(3)−As(1)−C(6)	97.6(3)	C(4)−As(2)−C(5)	93.6(3)
As−C═C[b]	As(1)−C(3)−C(4)	116.7(5)	As(1)−C(6)−C(5)	116.7(5)
As−C═C[c]	As(2)−C(4)−C(3)	122.1(5)	As(2)−C(5)−C(6)	122.7(5)
I−Pt−I	I(1)−Pt(1)−I(1)	180.00(2)		
As−Pt−As	As(1)−Pt(1)−As(1)	180.00(2)		
torsion angle	I(1)−Pt(1)−As(1)−C(1)	80.1(3)		

[a]Interior angle of the six-membered ring. [b]Bond angles of the coordinated side. [c]Bond angles of the vacant arsenic.

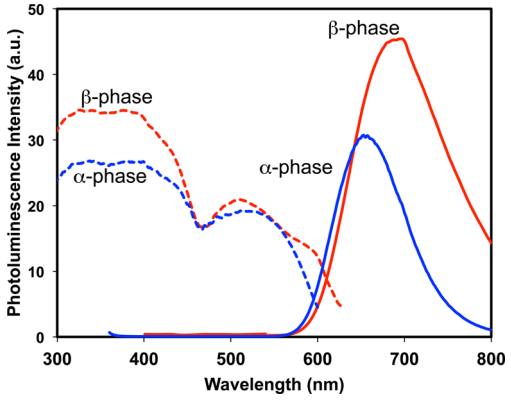

Figure 3. Room-temperature excitation (dashed blue line and dashed red line, upon emission at λ = 635 and 650 nm, respectively) and emission (solid blue and red lines, upon excitation at λ = 350 nm) spectra of the α- and β-phase crystals in the solid state.

groups on the coordinated arsenic atoms in the crystals due to the restricted crystal packing is most likely responsible for enhancement of the emission at room temperature.

The lifetime decays for both luminescent crystals are monoexponential, in the microsecond region, suggesting that the emission occurs from only one excited state (Supporting Information, Figure S4). Radiative and nonradiative deactivation rate constants were calculated from the luminescence lifetimes and quantum yields (Table 2).[12] Although the radiative deactivation rate constants (k_r^T) for the α- and β-phases are similar, the nonradiative deactivation rate constant (k_{nr}^T) of the β-phase is 1 order of magnitude higher than that of the α-phase, indicating that the α-phase predominantly prevents the nonradiative relaxation process in comparison with the β-phase. In the crystal packing of the α-phase, the methyl groups on the coordinated arsenic atoms are connected to the methyl groups on the uncoordinated arsenic atom of adjacent molecules. On the other hand, the methyl groups on the coordinated arsenic atoms in the crystal packing of the β-phase crystals are connected to the methyl groups of the methoxycarbonyl substituent of adjacent molecules (Supporting Information, Figure S6). These observations suggest that the molecular motion of the six-membered ring of cis-DHDAMe in the α-phase crystals is more directly restricted than that in the β-phase crystals. In addition, the short H−H distance (2.276 Å) of the methyl groups on the coordinated arsenic atoms in the crystal packing of the α-phase with the adjacent methyl group is shorter than that of the β-phase (2.335 Å). These results suggest that degree of the freezing of the intramolecular rotational relaxation pathways of the six-membered ring of *cis*-DHDAMe in the crystals is most likely responsible for enhancement of the luminescence quantum yield at room temperature.

After heating the α-phase crystals at 150 °C for 2 min, however, a powder XRD pattern different from that of the original crystal is obtained (Figure 5a,b), and its solid-state emission at room temperature decreased (λ_{em} = 650 nm, Φ = 0.03). After heating the β-phase crystals at 150 °C for 2 min, the emission wavelength and the quantum yield of the solid-

dx.doi.org/10.1021/ic500550y | Inorg. Chem. 2014, 53, 8270−8277

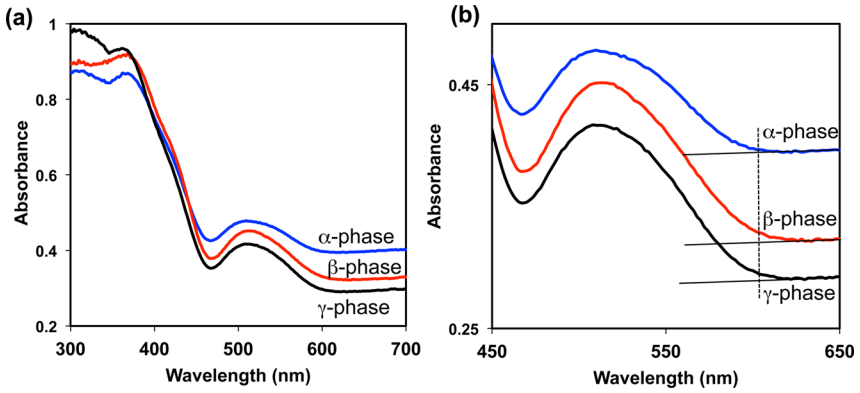

Figure 4. (a) Solid-sate optical absorption spectra for the α-, β-, and γ-phase crystals at room temperature and (b) expanded area.

Table 2. Emission Data for the α-Phase and β-Phase Crystals in the Solid State at Room Temperature

sample	λ_{em}[a] [nm]	τ_{em} [μs]	Φ	k_r^T ($\times 10^{-4}$ s^{-1})	k_{nr}^T ($\times 10^{-4}$ s^{-1})
α-phase	657	29	0.52	1.8	1.7
β-phase	695	6.8	0.09	1.3	15

[a]Abbreviations: λ_{em} = emission maximum (λ_{ex}= 350 nm), τ_{em} = lifetime, Φ = fluorescence quatum yield determined using a calibrated integrating sphere, k_r^T = radiative deactivation rate constant, k_{nr}^T = nonradiative deactivation rate constant.

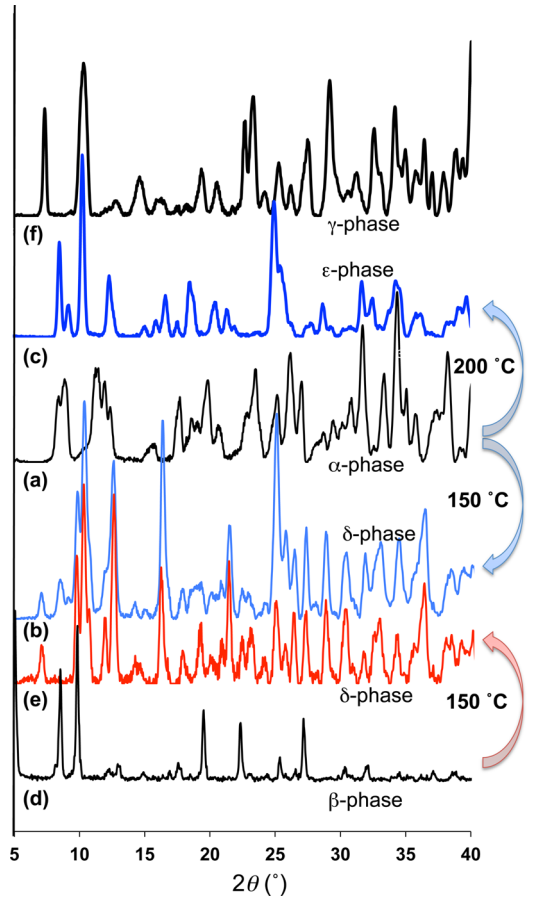

Figure 5. Powder XRD patterns of the α-phase before (a) and after (b) heating at 150 °C and 200 °C (c), the β-phase before (d) and after (e) heating at 150 °C, and the γ-phase (f).

state emission at room temperature (λ_{em} = 655 nm, Φ = 0.03) and the powder XRD pattern are the same as those of the α-phase after heating at 150 °C (Figure 5d,e). These transitions are irreversible. These results suggest that a crystal-to-crystal transition triggered by the thermal stimulus at 150 °C for the crystals of both α- and β-phase produces the same polymorph (δ-phase) of the mononuclear diiodoplatinum(II) complex. Differential scanning calorimetry (DSC) curves obtained for the crystals of α- and β-phase showed clear single endothermic peaks at 138 and 120 °C, respectively, corresponding to the crystal transitions to δ-phase (Figure 6). In addition, the α- and β-phase crystals show relatively weak endothermic peaks at 184 and 178 °C, respectively. No endothermic peaks can be observed during the second heating of either crystal. After

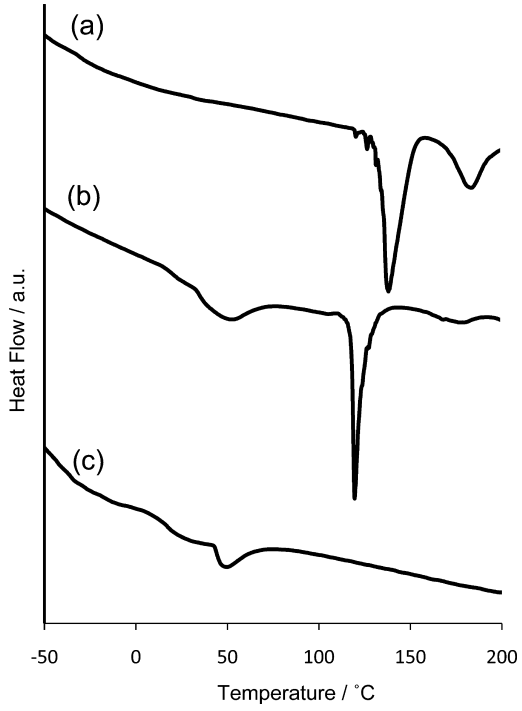

Figure 6. Differential scanning calorimetry (DSC) curves of the crystals of (a) α-, (b) β-, and (c) γ-phases at a heating rate of 10 °C/min in N_2 flow for the whole temperature range.

dx.doi.org/10.1021/ic500550y | Inorg. Chem. 2014, 53, 8270−8277

heating the α-phase crystals at 200 °C for 2 min, a powder XRD pattern different from the original crystals before (α-phase) and after heating at 150 °C (δ-phase) is obtained (Figure 5c). The obtained crystals show no solid-state luminescence at room temperature. The powder XRD pattern is, however, different from that of the γ-phase crystals (Figure 5f). This result suggests that a new polymorph (ε-phase) is produced by the thermal stimulus at 200 °C. The crystals of β- and γ-phase crystals show weak and broad endothermic peaks at ~50 °C, which might be derived from desorption of solvent molecules. The powder XRD patterns of the β- and γ-phase crystals after heating at 110 and 100 °C for 2 min, respectively, match those of the original crystals (Supporting Information, Figures S7 and S8).

The crystals of β-phase were exposed to I_2 vapors to test their readsorption capabilities. Exposure of the sample was carried out in a closed chamber. The colorless crystals turned dark brown within a few hours. The iodine sublimed into the porous crystals over time at ambient temperature, and this was apparent from a color change in the crystal from red-orange to almost black. Gravimetric measurements were taken at various time intervals during the iodine loading after the crystals were placed under reduced pressure at room temperature to remove weakly absorbed iodine at the surfaces. The rate of mass increase was slow as the pores became more occupied with the iodine guest and saturated at 8 wt %, that is, 0.43 iodine molecules per cage molecule, after 38 h (Figure 7). According

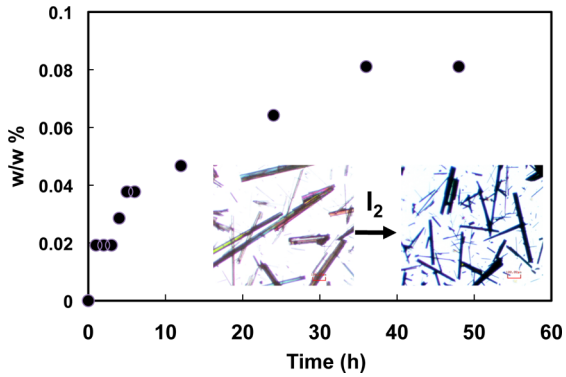

Figure 7. Gravimetric uptake of iodine as a function of time at room temperature. (inset) Optical microscopic images for the β-phase crystals before and after exposure to iodine vapor.

to this value, an axial length of an iodine molecule against a 1D nanochannel is 6.2 Å, which is slightly shorter than the major diameter of iodine molecule (6.8 Å). The XRD pattern after exposing to iodine vapor shows the same XRD pattern before exposing to iodine vapor except a new peak at $2\theta = 7.1°$, which corresponds to the distance of two iodine molecules (12.4 Å) in the 1D nanochannel. The unit cell parameters of I_2-absorbed crystals determined by XRD analysis indicated no change in their crystal structure (Figure 8b). No solid-state emission was observed for the black crystals. No removal of iodine was observed when the crystals were placed under reduced pressure at room temperature. Washing the I_2-absorbed crystal with methanol led to the removal of I_2, and the crystals slowly turned back to their original color. The washed crystals showed the same solid-state emission and diffraction pattern of the initial crystals (Figure 8c).

In summary, we have shown that *trans*-PtI_2(*cis*-DHDAMe)$_2$ forms at least four crystalline polymorphs. The present unique

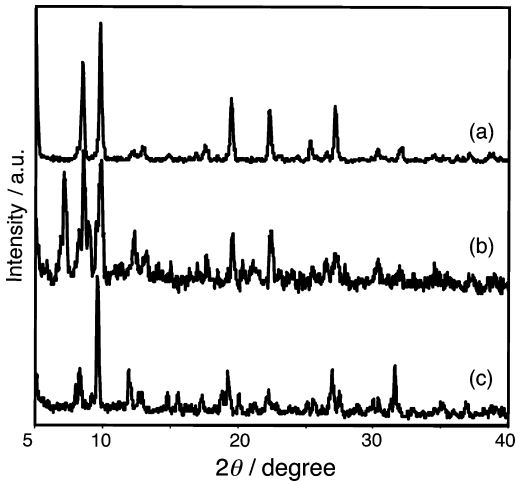

Figure 8. Powder XRD patterns of the β-phase crystals before (a) and after (b) exposure to iodine vapor, and removing iodine by washing with methanol (c).

polymorphism might originate from the flexibility of the organoarsenic compounds. The different molecular packings in these crystals affect their solid-state emission properties. Thermal stimulation of the luminescent crystals produces different stable polymorphs by crystal-to-crystal transitions. Stable crystals having 1D nanochannels can be obtained as one of these polymorphs. The 1D porous crystals exhibit room-temperature solid-state luminescence properties, as a first example of luminescent single-metal complexes that form molecular crystals containing 1D nanochannels. Crystal structure of this phase (β-phase) was found to be stable at 110 °C. Guest molecules, such as iodine, are reversibly encapsulated in the 1D nanochannels without distorting the crystal packing. Such crystals showing open framework structures allow for sorption/desorption equilibrium of guest molecules, similar to inorganic zeolite channel-type crystals. Detailed optical and physical studies are now underway.

EXPERIMENTAL SECTION

Materials. Mononuclear dichloroplatinum(II) complex (*trans*-$PtCl_2$(*cis*-DHDAMe)$_2$) was obtained by complexation of *cis*-DHDAMe with a half-equimolar amount of $PtCl_2(PhCN)_2$ according to the previous report.

Synthesis of *trans*-PtI_2(*cis*-DHDAMe)$_2$. A mixture of the mononuclear dichloroplatinum(II) complex (*trans*-$PtCl_2$(*cis*-DHDAMe)$_2$)[11] (1.05 g, 0.882 mmol), which was obtained by complexation of *cis*-DHDAMe with a half-equimolar amount of $PtCl_2(PhCN)_2$, and KI (2.93 g, 17.7 mmol) in acetone (70 mL) was stirred at room temperature for 5 h and gave an orange solution. The solvent was removed in vacuo. The residue was dissolved in CH_2Cl_2, and KI precipitate was filtered off. The red-orange solution was recrystallized from CH_2Cl_2 and methanol to give a red-orange crystal. Yield: 85%. ^{1}H NMR ($CDCl_3$) δ: 3.83 (s, 2H); 3.80 (s, 2H); 2.42 (s, $^3J_{Pt-H}$ = 10 Hz, 1H), 1.36 (s, 1H). ^{13}C NMR ($CDCl_3$) δ: 166.62; 162.98; 156.19; 136.65; 53.16; 52.89; 16.67; 6.71. Anal. Calcd for $C_{28}H_{36}As_4Cl_2O_{16}Pt$: C, 24.42; H, 2.63; I, 18.43. found: C, 24.21; H, 2.68; I, 18.33%.

X-ray Crystallographic Data for Single Crystalline Products. The single crystal was mounted on glass fibers with epoxy resin. Intensity data were collected at room temperature on a Rigaku RAXIS RAPID II imaging plate area detector with graphite monochromated Mo Kα radiation. The crystal-to-detector distance was 127.40 mm. Readout was performed in the 0.100 mm pixel mode. The data were collected at room temperature to a maximum 2q value of 55.0°. Data were

dx.doi.org/10.1021/ic500550y | Inorg. Chem. 2014, 53, 8270−8277

Table 3. Selected Crystallographic Data and Refinement Parameters for the Crystalline Products

	α-phase	β-phase	γ-phase
empirical formula	$C_{28}H_{36}O_{16}As_4PtI_2$	$C_{28}H_{36}O_{16}As_4PtI_2$	$C_{28}H_{36}O_{16}As_4PtI_2$
formula weight	1377.17	1377.17	1377.17
crystal system	triclinic	trigonal	orthorhombic
space group	$P\bar{1}$	$R\bar{3}$	*Pbca*
a (Å)	9.5639(4)	36.9198(19)	13.9226(5)
b (Å)	10.4571(3)	36.9198(19)	12.4426(4)
c (Å)	11.3354(4)	8.22428(19)	24.7967(7)
α (deg)	86.8846(9)	90.0000	90.0000
β (deg)	70.9998(12)	90.0000	90.0000
γ (deg)	71.6438(12)	120.0000	90.0000
V (Å^3)	1015.89(6)	9708.4(8)	4295.6(2)
Z	1	9	4
D_{calcd} (g cm^{-3})	2.251	2.120	2.129
μ (mm^{-1})	8.257	7.776	7.811
T (K)	296	296	296
reflections collected	10 076	21 187	57 350
independent reflections (R_{int})	4607(0.035)	4927(0.0910)	4909(0.093)
observed reflections [$I > 2\sigma(I)$]	3297	4927	2873
parameters	250	232	250
T_{min}/T_{max}	0.451/0.609	0.481/0.733	0.266/0.310
residual density (eÅ^{-3})	0.94/−0.68	0.95/−0.66	2.21/−0.99
R_1	0.0294	0.0440	0.0317
wR_2	0.0667	0.0864	0.0639
GOF	1.007	1.031	1.021

processed by the PROCESS-AUTO[13] program package. An empirical or numerical absorption correction[14] was applied. The data were corrected for Lorentz and polarization effects. A correction for secondary extinction[15] was applied. The structure was solved by heavy-atom Patterson methods[16] and expanded using Fourier techniques.[17] Some non-hydrogen atoms were refined anisotropically, while the rest were refined isotropically. Hydrogen atoms were refined using the riding model. The final cycle of full-matrix least-squares refinement on F^2 was based on observed reflections and variable parameters. In the case of the crystalline product recrystallized from acetone, the final cycle of full-matrix least-squares refinement on *F* was based on observed reflections and variable parameters. All calculations were performed using the CrystalStructure[18,19] crystallographic software package. Crystal data and more information on X-ray data collection are summarized in Table 3.

Measurements. X-ray diffraction (XRD) was recorded on a Smart Lab (Rigaku) with Cu Kα radiation (λ = 1.5406 Å) in θ/2θ mode at room temperature. The 2θ scans were collected at 0.01° intervals, and the scan speed was 2°(2θ)/min. ^{1}H (300 or 400 MHz) and ^{13}C (75 and 100 MHz) NMR spectra were recorded on a Bruker PDX-300. UV−vis spectra were recorded on a JASCO spectrophotometer V-670 KKN. Differential scanning calorimetry (DSC) was recorded on a TA Instruments 2920 Modulated DSC. Elemental analysis was performed at the Microanalytical Center of Kyoto University. Emission and excitation spectra were obtained on an FP-8500 (JASCO). The luminescence decay time of the crystalline solid was obtained using a least-squares method for time courses of luminescence recorded by a correlated single-photon counting method using a femtosecond Ti^{3+}:sapphire laser (400 nm) with a cavity dumper (~10 kHz).[20]

■ ASSOCIATED CONTENT

Supporting Information

^{1}H NMR spectra, comparison of the I−Pt−As-C torsion angles and the crystal packing of the α-phase, β-phase and γ-phase crystals, emission decays, additional XRD data, and CIF files. This material is available free of charge via the Internet at http://pubs.acs.org.

■ AUTHOR INFORMATION

Corresponding Author

*E-mail: kenaka@kit.ac.jp.

Notes

The authors declare no competing financial interest.

■ ACKNOWLEDGMENTS

This work was supported by Grant-in-Aid for Scientific Research (No. 20350054) from the Ministry of Education, Culture, Sports, Science, and Technology, Government of Japan and partially supported by the Asahi Glass Foundation. We thank Prof. N. Ikeda of KIT for estimating the luminescence decay time.

■ REFERENCES

(1) (a) Braga, D.; Grepioni, F.; Maini, L. *Chem. Commun.* **2010**, *46*, 6232−6242. (b) Braga, D.; Grepioni, F. *Chem. Soc. Rev.* **2000**, *29*, 229−238. (c) Braga, D.; Grepioni, F. *Acc. Chem. Res.* **2000**, *33*, 601−608.

(2) Hiremath, R.; Basile, J. A.; Varney, S. W.; Swift, J. A. *J. Am. Chem. Soc.* **2005**, *127*, 18321−18327.

(3) (a) Ito, H.; Muromoto, M.; Kurenuma, S.; Ishizaka, S.; Kitamura, N.; Sato, H.; Seki, T. *Nat. Commun.* **2013**, *4*, 2009. (b) Mutai, T.; Satou, H.; Araki, K. *Nat. Mater.* **2005**, *4*, 685−687. (c) Campione, M.; Tavazzi, S.; Moret, M.; Porzio, W. *J. Appl. Phys.* **2007**, *101*, 083512.

(4) (a) Procopio, E. Q.; Mauro, M.; Panigati, M.; Donghi, D.; Mercandelli, P.; Sironi, A.; D'Alfonso, G.; De Cola, L. *J. Am. Chem. Soc.* **2010**, *132*, 14397−14399. (b) Zhang, H. Y.; Zhang, Z. L.; Ye, K. Q.; Zhang, J. Y.; Wang, Y. *Adv. Mater.* **2006**, *18*, 2369−2372. (c) Luo, G. G.; Xia, J. X.; Fang, K.; Zhao, Q. H.; Wu, J. H.; Dai, J. C. *Dalton Trans.* **2013**, *42*, 16268−16271.

(5) (a) Allcock, H. R.; Levin, M. L.; Whittle, R. R. *Inorg. Chem.* **1986**, *25*, 41−47. (b) Sozzani, P.; Comotti, A.; Simonutti, R.; Meersmann, T.; Logan, J. W.; Pines, A. *Angew. Chem., Int. Ed.* **2000**, *39*, 2695−2698. (c) Hertzsch, T.; Kluge, S.; Weber, E.; Buddle, F.; Hulliger, J. *Adv. Mater.* **2001**, *13*, 1864−1867. (d) Hertzsch, T.; Budde, F.; Weber,

E.; Hulliger, J. *Angew. Chem., Int. Ed.* **2002**, *41*, 2281−2284. (e) Sozzani, P.; Bracco, S.; Comotti, A.; Ferretti, L.; Simonutti, R. *Angew. Chem., Int. Ed.* **2005**, *44*, 1816−1820. (f) Kobayashi, H.; Ueda, T.; Miyakubo, K.; Eguchi, T.; Tani, A. *Bull. Chem. Soc. Jpn.* **2007**, *80*, 711−720. (g) Kobayashi, H.; Takeuchi, K.; Asaji, T. *J. Phys. Chem. A* **2013**, *117*, 2093−2101.

(6) (a) Zhou, H.; Long, J. R.; Yaghi, O. M. *Chem. Rev.* **2012**, *112*, 673−674. (b) Kitagawa, S.; Kitaura, R.; Noro, S. *Angew. Chem., Int. Ed.* **2004**, *43*, 2334−2375.

(7) Yin, Z.; Wang, Q.-X.; Zeng, M.-H. J. *J. Am. Chem. Soc.* **2012**, *134*, 4857−4863.

(8) Martí-Rujas, J.; Colombo, L.; Lü, J.; Dey, A.; Terraneo, G.; Metrangolo, P.; Pilati, T.; Resnati, G. *Chem. Commun.* **2012**, *48*, 8207−8209.

(9) (a) Natarajan, R.; Bridgland, L.; Sirikulkajorn, A.; Lee, J.-H.; Haddow, M. F.; Magro, G.; Ali, B.; Narayanan, S.; Strickland, P.; Charmant, J. P. H.; Orpen, A. G.; McKeown, N. B.; Bezzu, C. G.; Davis, A. P. *J. Am. Chem. Soc.* **2013**, *135*, 16912−16925. (b) Rajput, L.; Chernyshevb, V. V.; Biradha, K. *Chem. Commun.* **2010**, *46*, 6530−6532.

(10) Naka, K.; Kato, T.; Watase, S.; Matsukawa, K. *Inorg. Chem.* **2012**, *51*, 4420−4422.

(11) Arita, M.; Naka, K.; Shimamoto, T.; Yumura, T.; Nakahashi, A.; Morisaki, Y.; Chujo, Y. *Organometallics* **2010**, *29*, 4992−5003.

(12) Valeur, B. *Molecular Fluorescence, Principles and Applications;* Wiley-VCH: Weinheim, Germany, 2002.

(13) *PROCESS-AUTO, RAXIS data-processing software;* Rigaku Corporation: Tokyo, Japan, 1996.

(14) Higashi, T. *FS_ABSCOR, Program for Absorption Correction;* Rigaku Corporation: Tokyo, Japan, 1995.

(15) Larson, A. C. *Crystallographic Computing;* Ahmed, F. R., Ed.; Munksgaard: Copenhagen, Denmark, 1970; pp 291−294.

(16) Beurskens, P. T.; Admiraal, G.; Beurskens, G.; Bosman, W. P.; de Gelder, R.; Israel, R.; Smits, J. M. M. *The DIRDIF-99 Program System;* Technical Report of the Crystallography Laboratory, University of Nijmegen: Nijmegen, The Netherlands, 1999.

(17) Beurskens, P. T.; Admiraal, G.; Beurskens, G.; Bosman, W. P.; Garcia-Granda, S.; Gould, R. O.; Smits, J. M. M.; Smykalla, C. *PATTY, The DIRDIF Program System;* Technical Report of the Crystallography Laboratory, University of Nijmegen: Nijmegen, The Netherlands, 1992.

(18) *CrystalStructure 3.8: Crystal Structure Analysis Package;* Rigaku Americas: The Woodlands, TX, 2000.

(19) Carruthers, J. R.; Rollett, J. S.; Betteridge, P. W.; Kinna, D.; Pearce, L.; Larsen, A.; Gabe, E. *CRYSTALS Issue 11;* Chemical Crystallography Laboratory: Oxford, U.K., 1999.

(20) Ohno, T.; Nozaki, K.; Nakamura, M.; Motojima, Y.; Tsushima, M.; Ikeda, N. *Inorg. Chem.* **2007**, *46*, 8859−8870.